An Active-Rectifier-Based Maximum Efficiency Tracking Method Using an Additional Measurement Coil for Wireless Power Transfer

Ruikun Mai, *Member, IEEE*, Yeran Liu, *Student Member, IEEE*, Yong Li, *Student Member, IEEE*, Pengfei Yue, Guangzhong Cao, *Member, IEEE*, and Zhengyou He, *Senior Member, IEEE*

***Abstract*—The efficiency of wireless power transfer (WPT) systems is highly dependent on the load, which may change in a wide range in field applications. Besides, the detuning of WPT systems caused by the component tolerance and aging of inductors and capacitors can also decrease the system efficiency. In order to track the maximum system efficiency under varied loads and detuning conditions in real time, an active single-phase rectifier (ASPR) with an auxiliary measurement coil (AMC) and its corresponding control method are proposed in this paper. Both the equivalent load impedance and the output voltage can be regulated by the ASPR and the inverter, separately. First, the fundamental harmonic analysis model is established to analyze the influence of the load and the detuning on the system efficiency. Second, the soft-switching conditions and the equivalent input impedance of ASPR with different phase shifts and pulse widths are investigated in detail. Then, the analysis of the AMC and the maximum efficiency control strategy are provided in detail. Finally, an 800-W prototype is set up to validate the performance of the proposed method. The experimental results show that with 10% tolerance of the resonant capacitor in the receiver side, the system efficiency with the proposed approach reaches 91.7% at rated 800-W load and 91.1% at 300-W light load, which has an improvement by 2% and 10% separately compared with the traditional diode rectifier.**

***Index Terms*—Active rectifier, maximum efficiency point track (MEPT), measurement coil, phase shift, wireless power transfer (WPT).**

I. Introduction

WIRELESS power transfer (WPT) technology has the advantage of canceling the twisted electrical wires by transferring energy through a relatively large air gap with magnetic field [1]. In recent years, the WPT technology based on electromagnetic coupling has been attracting many researchers' attentions and widely adopted throughout the world. With the merit of safety and convenience, it has been applied to many applications, such as biomedical plant [2], underwater equipment [3], mobile phone [4], electrical vehicles [5]–[9], and even the trains [10], [11]. The power levels of WPT systems range from milliwatt [12] to megawatt [11].

Overall efficiency of a WPT system is one of the most important performances concerned by the public, especially for the high-power-level applications [13]. Some optimal methods, such as compensation parameter optimization [14], optimizable circuit structure [15], and operating frequency selection [16], have been proposed to improve the efficiency under some circumstances. However, the equivalent resistance of the load, for example, the battery, can go from 3.6 to 560 Ω dependent on its charging profile [17]. The various equivalent loads for WPT systems affect the overall efficiency dramatically. Moreover, the tolerance of components can also influence the system efficiency. Therefore, a WPT system without feedback control is hard to maintain a high overall efficiency all the time.

To address this problem, the active maximum efficiency point tracking (MEPT) method has been proposed to overcome the variation of load resistance. Generally, these methods employ power electronic converters, such as semibridge rectifier [18], full-bridge rectifier [19], dc/dc converters [20]–[23], etc., to achieve the maximum efficiency by altering the equivalent load resistance in real time with the assumption that the WPT system is completely tuned. These methods can roughly be divided into two categories: 1) model-based approaches [18]–[20]; and 2) "perturb-and-observe" (P&O)-based approaches [21]–[23]. For the model-based approaches, the maximum efficiency is achieved by adjusting the pulse width of the semibridge rectifier [18], [19] or the conduction angle of the dc/dc converter [20] according to the mathematic models on circuit parameters and efficiency. For the P&O approaches, a dc/dc converter in the transmitting side [21], [22] or in the receiver side [21], [23] is used to search for the maximum efficiency point by perturbing the conduction angle of the converter, calculating the efficiency and then updating the perturbation direction.

Most of the researches mentioned above are based on the ideal resonant condition of WPT systems, but it is difficult to guarantee that it is true under various working conditions in practice. Due to the component tolerance and aging of the inductors and capacitors in severe conditions, the circuitry parameters may

Manuscript received September 7, 2016; revised December 2, 2016; accepted January 23, 2017. Date of publication February 6, 2017; date of current version October 6, 2017. This work was supported in part by the National Natural Science Foundation of China under Grant 51507147, in part by the National Natural Science Foundation of China under Grant 51677155, and in part by the National Science Fund for Distinguished Young Scholars under Grant 51525702. Recommended for publication by Associate Editor S.-C. Tan.

R. Mai, Y. Liu, Y. Li, P. Yue, and Z. He are with the School of Electrical Engineering, Southwest Jiaotong University, Chengdu 610031, China (e-mail: mairk@swjtu.edu.cn; leeo1864@163.com; yeranliu@my.swjtu.edu.cn; yuepengfei_yf@163.com; hezy@swjtu.edu.cn).

G. Cao is with the Shenzhen Key Laboratory of Electromagnetic Control, Shenzhen University, Shenzhen 518060, China (e-mail: gzcao@szu.edu.cn).

Color versions of one or more of the figures in this paper are available online at http://ieeexplore.ieee.org.

Digital Object Identifier 10.1109/TPEL.2017.2665040

slightly drift away from the nominal one and the system would detune afterward. The reactance mismatch caused by detuning can have great influence on the system output power and efficiency so that the performance of the overall system will degrade accordingly. In order to adjust the load reactance and tune the system's resonance, the capacitor arrays are utilized in [24] and [25] by switching the connection of the capacitors so that the system can be maintained resonant. These methods can, then, improve the system efficiency.

As the approaches mentioned above just have one degree of control freedom, either the equivalent resistance or the reactance of the overall system can be regulated. Therefore, the maximum efficiency point cannot be maintained under load variation conditions and reactance mismatch conditions. In order to overcome this drawback, another degree of freedom should be added to the control method to track the maximum efficiency point by altering the equivalent load reactance and resistance, simultaneously. In [26], a phase-shift control of a semibridge rectifier is proposed. The equivalent impedance related to the pulse width and the phase shift of the semibridge rectifier is derived. With this method, the output voltage of the system can be regulated without communication between the receiver and transmitter. In [19], a method that controls the phase shift of the active rectifier and its output voltage level to adjust the load impedance is proposed to improve the system efficiency. Two degree freedoms of the control strategy, the pulse width and the phase shift of the rectifier, are employed to adjust the load reactance and resistance. This method does improve the overall efficiency of the WPT system with the assumption that the coupling coefficient and the drift reactance are known beforehand. The pulse width and phase shift angle can be solved offline and then the results can be implemented online to improve the efficiency with the help of optimization methodology. Both [19] and [26] provide useful methods to change the equivalent impedance of active rectifier and supply topologies with two one degrees of control freedom for the MEPT, but how to measure and calculate the reactance that should be compensated under nonresonance condition and how to track the maximum efficiency point under various conditions in real time need to be further investigated.

In this paper, an active single-phase rectifier (ASPR) with an auxiliary measurement coil (AMC) and a corresponding control method are proposed for the MEPT in various conditions, such as reactance mismatch conditions and various load resistance conditions. Owing to the AMC circuit and a decoupling transformer, the phase of induced voltage in the receiver side can be measured directly and then the resonant condition is able to be criticized by calculating the phase difference between the induced voltage and the receiver current. In addition, a MEPT control method is proposed to maximize the system efficiency for reactance mismatch and varied loads in real time. With the property of ASPR, a decoupled control of the equivalent load resistance and reactance can be achieved by applying the conduction angle and phase-shift strategy of ASPR. This control method can not only cancel the reactance of the receiver side caused by component tolerance, but also adjust the equivalent load resistance to be the optimal value for maximum efficiency.

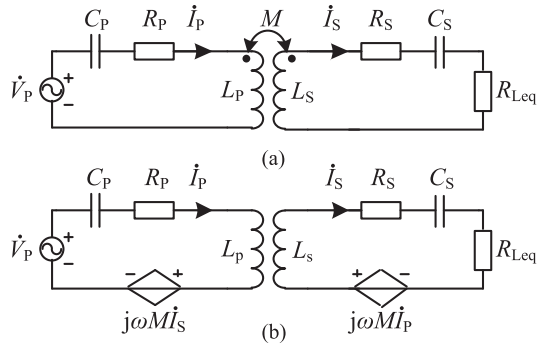

Fig. 1. Fundamental harmonic analysis model of a typical SS topology-based IPT system and its equivalent decoupling circuit. (a) Fundamental harmonic analysis model. (b) Equivalent circuit.

Meanwhile, the output voltage can be regulated by changing the pulse width of the power supply inverter.

This paper is organized as follows: Section II analyzes the output voltage and system efficiency based on the fundamental harmonic analysis model of the WPT system. Section III describes the soft-switching conditions and analyzes the equivalent input impedance of ASPR. The tuning principle based on AMC and the MEPT control method is proposed in Section IV and validated by experiments in Section V. Finally, the conclusion is drawn in Section VI.

II. Theoretical Analysis

A. System Modeling

In order to analyze the circuit characteristic, the fundamental-harmonic analysis model of a series–series (SS) compensation topology-based WPT system is employed, as shown in Fig. 1(a). The voltage source $\dot{V}_P$ is assumed to be sinusoidal with the angular frequency ω and the transmitter's current $\dot{I}_P$ is fed into the resonant tank to energize the transmitter coil. Then, the power is transferred from the transmitter to the receiver through a loosely coupling transformer with the coupling coefficient of $k = M/\sqrt{L_P L_S}$, where L_P, L_S, and M are the transmitter's inductance, the receiver's inductance, and their mutual inductance. C_P and C_S are resonant capacitors adopted to compensate L_P and L_S. The equivalent-series resisters (ESR) of the coils R_P and R_S are taken into account for the purpose of analyzing the efficiency with the assumption that R_P and R_S are not changed with ambience temperature. R_{Leq} is the equivalent ac load resister that stands for the input resistance of the high-frequency rectifier.

For the convenience of analysis, the transmitter and the receiver are decoupled by adding two current-controlled voltage sources, as shown in Fig. 1(b). According to the Kirchhoff's voltage law, the system can be described by the following equations:

$$\begin{cases} \dot{V}_P = Z_P \dot{I}_P + j\omega M \dot{I}_S \\ 0 = j\omega M \dot{I}_P + Z_S \dot{I}_S + R_{Leq} \dot{I}_S \end{cases}. \tag{1}$$

TABLE I
PARAMETERS OF THE WPT SYSTEM FOR ANALYSIS

Symbol	Parameter	Value	Unit
f	Inverter frequency	30	kHz
R_{P}	Transmitter coil ESR	0.1	Ω
L_{P}	Transmitter coil inductance	252	μH
R_{S}	Receiver coil ESR	0.1	Ω
L_{S}	Receiver coil inductance	246	μH
M	Mutual inductance of transmitter and receiver side coils	46.32	μH
R_{Leq}	Equivalent ac load resister	[5, 10 000]	Ω
X_{S}	Reactance in the receiver side	[−10, 10]	Ω

According to the circuitry analysis, the impedance of the transmitter and receiver are given by

$$\begin{cases} Z_{\mathrm{P}} = j\omega L_{\mathrm{P}} + (j\omega C_{\mathrm{P}})^{-1} + R_{\mathrm{P}} = jX_{\mathrm{P}} + R_{\mathrm{P}} \\ Z_{\mathrm{S}} = j\omega L_{\mathrm{S}} + (j\omega C_{\mathrm{S}})^{-1} + R_{\mathrm{S}} = jX_{\mathrm{S}} + R_{\mathrm{S}} \end{cases} \tag{2}$$

where ω is the operating angular frequency. X_{P} (X_{S}) is the equivalent impedance of transmitter's (receiver's) inductance and capacitor. When the transmitter (receiver) is under resonant condition, X_{P} (X_{S}) is equal to zero and the transmitter (receiver) side is fine tuned.

B. Output Voltage Gain Analysis

By substituting (2) into (1), the currents of the transmitter and the receiver can be derived accordingly as follows:

$$\begin{aligned} \dot{I}_{\mathrm{P}} &= \dot{V}_{\mathrm{P}} \left(N_{\mathrm{PR}} + jN_{\mathrm{PI}}\right)/D_{\mathrm{P}} \\ \dot{I}_{\mathrm{S}} &= \dot{V}_{\mathrm{P}} \left(N_{\mathrm{SR}} + jN_{\mathrm{SI}}\right)/D_{\mathrm{P}} \end{aligned} \tag{3}$$

where

$$\begin{aligned} N_{\mathrm{PR}} &= M^2\omega^2 \left(R_{\mathrm{S}} + R_{\mathrm{Leq}}\right) + R_{\mathrm{P}} \left[\left(R_{\mathrm{S}} + R_{\mathrm{Leq}}\right)^2 + X_{\mathrm{S}}^2\right] \\ N_{\mathrm{PI}} &= -X_{\mathrm{P}}\left(R_{\mathrm{S}} + R_{\mathrm{Leq}}\right)^2 + M^2\omega^2 X_{\mathrm{S}} - X_{\mathrm{P}} X_{\mathrm{S}}^2 \\ N_{\mathrm{SR}} &= M\omega(R_{\mathrm{P}} X_{\mathrm{S}} + R_{\mathrm{S}} X_{\mathrm{P}} + X_{\mathrm{P}} R_{\mathrm{Leq}}) \\ N_{\mathrm{SI}} &= M\omega(X_{\mathrm{P}} X_{\mathrm{S}} - \omega^2 M^2 - R_{\mathrm{P}} R_{\mathrm{S}} - R_{\mathrm{P}} R_{\mathrm{Leq}}) \\ D_{\mathrm{P}} &= \left(X_{\mathrm{P}}^2 + R_{\mathrm{P}}^2\right) \left[\left(R_{\mathrm{S}} + R_{\mathrm{Leq}}\right)^2 + X_{\mathrm{S}}^2\right] + 2M^2\omega^2 \\ &\quad \times \left(-X_{\mathrm{P}} X_{\mathrm{S}} + R_{\mathrm{P}} R_{\mathrm{Leq}} + R_{\mathrm{P}} R_{\mathrm{S}} + M^2\omega^2/2\right). \end{aligned} \tag{4}$$

The voltage gain is denoted by the ratio of the output voltage and the input voltage as follows:

$$G_{\mathrm{VV}} = R_{\mathrm{Leq}} \dot{I}_{\mathrm{S}}/\dot{V}_{\mathrm{P}} = R_{\mathrm{Leq}} \left(N_{\mathrm{SR}} + jN_{\mathrm{SI}}\right)/D_{\mathrm{P}}. \tag{5}$$

In this paper, an ASPR with an AMC and a corresponding control method are proposed for the MEPT in various conditions, such as reactance mismatch conditions and various load resistance conditions. Owing to the AMC circuit and with the system parameters listed in Table I, the voltage gain G_{VV} against $R_{\mathrm{Leq}}$and X_{S} is plotted in Fig. 2 to illustrate the effect of the two coresponding variables $R_{\mathrm{Leq}}$and X_{S} on the voltage gain. R_{Leq} varies from 5 Ω to 10 000 Ω. X_{P} is set to be zero. X_{S} indicating the nonresonance condition in the receiver side is set in the range from −10 Ω to 10 Ω. The voltage gain G_{VV} becomes larger as R_{Leq} increases in a wide range. When R_{Leq} is larger than 10 000 Ω, G_{VV} gradually approach to a limited constant value.

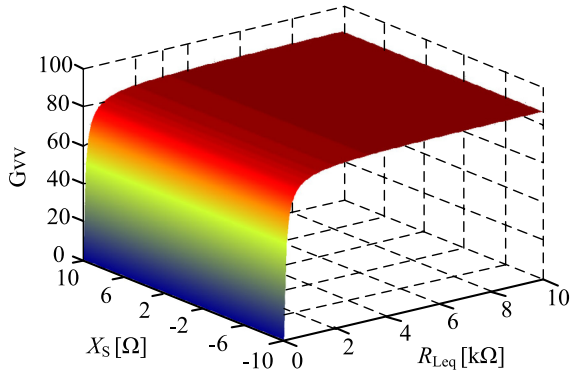

Fig. 2. Voltage gain G_{VV} against equivalent load R_{Leq} and reactance X_{S} in the receiver side.

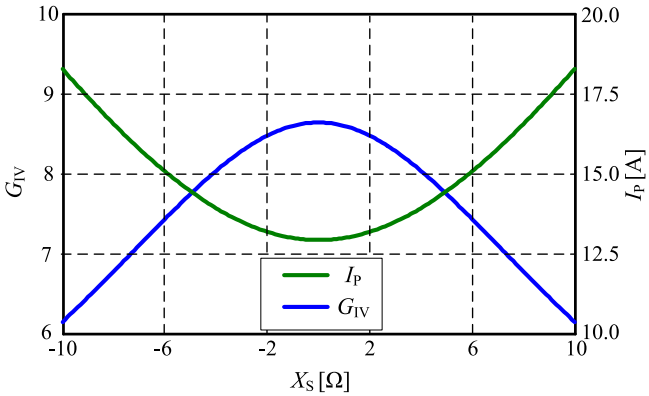

Fig. 3. Transmitter current I_{P} and current–voltage gain G_{IV} against X_{S}.

The effect of X_{S} on the voltage–voltage gain is not apparent, as shown in Fig. 2, but the existence of X_{S} can increase the transmitter side' current I_{P} and the current–voltage gain G_{IV} of the system is decreased, as shown in Fig. 3. That is because the existence of X_{S} decreases the reflected impedance of the receiver in the transmitter side. If the input voltage is fixed, I_{P} will increase for largerX_{S}. However, I_{P} should be limited in order to protect the inverter, resonant capacitor, and transmitter coil. Therefore, for a given limitation of I_{P}, the output voltage of the system in resonance condition is larger than that of the system in nonresonance condition according to the G_{IV} in Fig. 3. If the load resister is fixed for a given limitation of I_{P}, the maximum output power is also larger in resonance condition than that in nonresonance condition. The compensation of receiver side's reactance X_{S} is of significance for the improvement of output voltage and power for a given limitation of transmitter side's current.

C. Maximum Efficiency

The input power and the output power can be derived from (1) and (3), respectively

$$\begin{aligned} P_{\mathrm{in}} &= \mathrm{Re}\left[\dot{V}_{\mathrm{P}} \cdot \left(\dot{I}_{\mathrm{P}}\right)^*\right] = \dot{V}_{\mathrm{P}} \dot{V}_{\mathrm{P}} N_{\mathrm{PR}}/D_{\mathrm{P}} \\ P_{\mathrm{out}} &= \mathrm{Re}\left[\dot{V}_{\mathrm{P}} \cdot \left(\dot{I}_{\mathrm{S}}\right)^*\right] = \dot{V}_{\mathrm{P}} \dot{V}_{\mathrm{P}} \omega^2 R_{\mathrm{Leq}}/D_{\mathrm{P}}. \end{aligned} \tag{6}$$

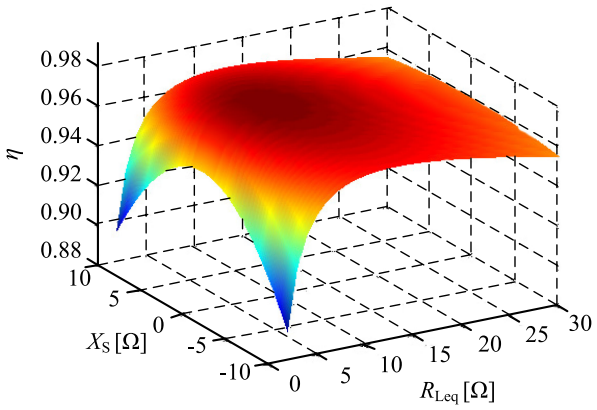

Fig. 4. System efficiency with equivalent load R_{Leq} and reactance X_{S} in the receiver side.

Then, the overall system's efficiency can be derived by the ratio of the input power and the output power

$$\eta = \frac{P_{\mathrm{out}}}{P_{\mathrm{in}}} = \frac{\omega^2 M^2 R_{\mathrm{Leq}}}{N_{\mathrm{PR}}} = \frac{\omega^2 M^2 R_{\mathrm{Leq}}}{M^2\omega^2 \left(R_{\mathrm{S}} + R_{\mathrm{Leq}}\right) + R_{\mathrm{P}}\left[\left(R_{\mathrm{S}} + R_{\mathrm{Leq}}\right)^2 + X_{\mathrm{S}}^2\right]}. \quad (7)$$

According to (7), the system efficiency has no relation to X_{P}, but it is a function against X_{S} and R_{Leq} asX_{S} is a part of the denominator of (7). It means that the larger the reactance of the receiver side is, the lower the system's efficiency will be. Therefore, $X_{\mathrm{S}}$is needed to be suppressed as much as possible in order to improve the system efficiency. With the parameters listed in Table I, the system efficiency as a function against X_{S} and R_{Leq} is calculated and plotted in Fig. 4. It is obvious that the system efficiency can go to maximum when X_{S} is eliminated for a given load resistanceR_{Leq}. Besides, there is an optimal load resistance for the maximum system's efficiency under the condition where $X_{\mathrm{S}} = 0$. The optimal load resistance, thus, can be solved by setting its derivative to be zero as follows:

$$\left.\frac{d\eta}{dR_{\mathrm{Leq}}}\right|_{X_{\mathrm{S}}=0} = 0. \quad (8)$$

Then, the optimal load resistance $R_{\mathrm{Leq}}^{\mathrm{opt}}$ is yielded as

$$R_{\mathrm{Leq}}^{\mathrm{opt}} = \sqrt{\frac{R_{\mathrm{S}}(M^2\omega^2 + R_{\mathrm{P}} R_{\mathrm{S}})}{R_{\mathrm{P}}}}. \quad (9)$$

$R_{\mathrm{Leq}}^{\mathrm{opt}}$ is the function against R_{P}, R_{S}, and M for a fixed operating frequency WPT system. The WPT system fails to maintain a high efficiency in all operating conditions as the equivalent load resistance deviates from the optimal one. As a result, not only the equivalent reactance of the receiver side should be eliminated, but also the equivalent ac equivalent resistance of the rectifier should be maintained to the optimal value as close as possible to achieve high efficiency.

It should be noted that R_{Leq} for the large voltage gain is different from the one for the maximum efficiency point according to Figs. 2 and 4. The value of G_{VV} is acceptable under the load resistance for the maximum efficiency point but a load resistance for high-voltage gain leads to low system efficiency which should be avoided. As discussed above, G_{VV} is related to R_{Leq}. A specific voltage gain under the maximum efficiency point can be achieved by setting the corresponding optimal load resistance, and the optimal load resistance can be adjusted by designing the mutual inductance M between the transmitter and receiver coil according to (9). Therefore, the specific voltage gain under the maximum efficiency point can be designed by adjusting the mutual inductance M, and more effort should be paid on the optimization of whole system efficiency under various load conditions for some applications.

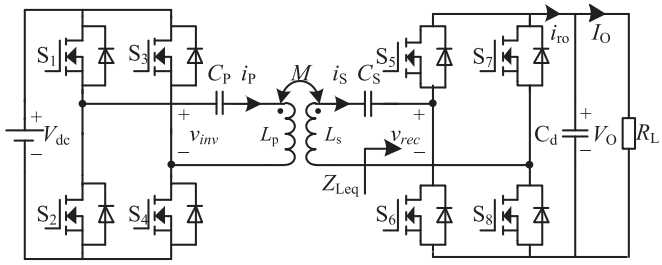

Fig. 5. Schematic of WPT system with ASPR.

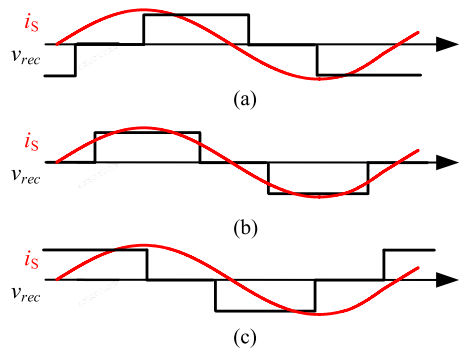

Fig. 6. Operating waveforms of receiver's current and the ASPR's voltage. (a) Situation A. (b) Situation B. (c) Situation C.

III. WPT System With ASPR

A. Circuit Analysis

The schematic of the WPT system with an ASPR is shown in Fig. 5. An ASPR-based control strategy is adopted to improve the performance of a WPT system by the pulse-width and phase-shift control against the receiver's current. The overall impedance of load is fully controlled by altering the pulse-width β of the ASPR and phase-shift φ between the first harmonic of the receiver's current and the input voltage of ASPR. Taking the receiver's current as reference, the operating waveforms of the receiver's current and the ASPR's voltage are presented in Fig. 6 to give the idea of the ASPR's behaviors with the following assumptions:

1) all the semiconductors are ideal without any parasitic resistance and capacitor;

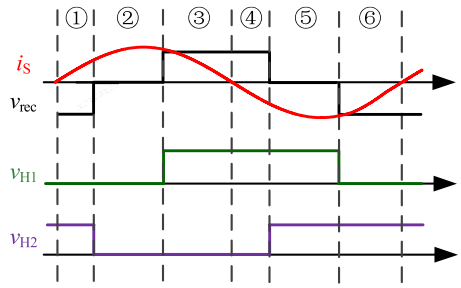

Fig. 7. Main waveforms of situation A in six modes.

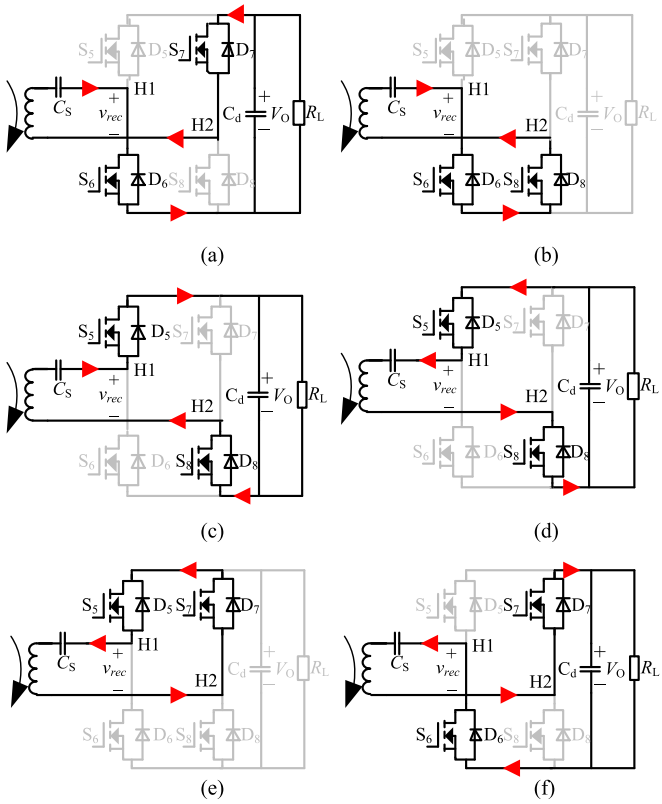

Fig. 8. Circuit analysis on six modes of situation A. (a) Mode ①. (b) Mode ②. (c) Mode ③. (d) Mode ④. (e) Mode ⑤. (f) Mode ⑥.

2) the voltage of the dc load bus remains constant.

As the ASPR is treated as a power receiver, the power goes into the ASPR instead of coming out so that the integration of the multiplication of current and voltage is supposed to be positive. As a consequence, there are three possible situations it may encounter with, as presented in Fig. 6.: 1) the voltage lags behind the current with the current crossing zero from positive to negative during the voltage pulse; 2) no matter the voltage leads or lags the current, the whole voltage pulse stays within the positive or negative current; and 3) the voltage leads the current with the current crossing zero from negative to positive during the voltage pulse.

Taking the situation 1 as an example, there are six following operation modes according to the operation of switches and the current direction, as shown in Figs. 7 and 8. v_{H1} and v_{H2} are the levels of the two points H1 and H2 of the ASPR, as shown in Fig. 7.

TABLE II
SOFT-SWITCHING ANALYSIS ON THREE OPERATING SITUATIONS OF THE ASPR

	Situation A	Situation B	Situation C
① to ②	HSOFFS_7	HSOFFS_6	SSOFFS_8
	SSONS_8	SSONS_5	HSONS_7
② to ③	HSOFFS_6	SSOFFS_8	SSOFFS_5
	SSONS_5	HSONS_7	HSONS_6
③ to ④	No action	No action	No action
④ to ⑤	HSOFFS_8	HSOFFS_5	SSOFFS_7
	SSONS_7	SSONS_6	HSONS_8
⑤ to ⑥	HSOFFS_5	SSOFFS_7	SSOFFS_6
	SSONS_6	HSONS_8	HSONS_5
⑥ to ①	No action	No action	No action
Summary		2 HSOFF	
	4 HSOFF	2 HSON	4 SSOFF
	4 SSON	2 SSOFF	4 HSON
		2 SSON	

Mode ①: During this interval, the switches S_6 and S_7 are turned ON. As shown in Fig. 4, the cycle starts with positive current I_S and negative voltage U_L. The current flows to the negative polarity of the load through S_6 and S_7. At that situation, the power is delivered from the load capacitor to the circuit. By hard–switching off S_7 and soft-switching on S_8, the mode ② comes.

Mode ②: The equivalent voltage of ASPR is shorted. The current flows through S_6 and antiparallel diode D_8 of S_8. At this state, no power flows into or out of the load capacitor. By hard-switching off S_6 and soft-switching on S_5, the mode ② comes.

Mode ③: Although the switches S_5 and S_8 are turned ON, the current flows into the load capacitor through the antiparallel diodes D_5 of S_5 and D_8 of S_8. No action is taken.

Mode ④: The current flows in negative polarity in this mode through switches S_5 and S_8. The power is extracted from the load capacitor again as the Mode ① does. By hard-switching off S_8 and soft-switching on S_7, the mode ⑤ comes.

Mode ⑤: The equivalent voltage of ASPR is shorted. The current flows through S_5 and antiparallel diode D_7 of S_7. At this stage, no power flows into or out of the load as Mode ① does. By hard-switching off S_5 and soft-switching on S_6, the mode ⑤ comes.

Mode ⑤: Although the switches S_6 and S_7 are turned ON, the current flows into the load capacitor through the antiparallel diodes D_6 of S_6 and D_7 of S_7. No action is taken. When the direction of the current reverses, the mode ⑤ comes.

During one cycle, four soft-switching on and four hard-switching off are required because the voltage lags the current. The whole cycle is operated under soft-switching condition and the switching loss is limited. However, the other two situations encounter with hard-switching on and the switching loss occurs, as shown in Table II. HSOFF (HSON) stands for hard-switching off (on), while SSOFF (SSON) stands for soft-switching off (on).

As a consequence, it is recommended to design the ASPR to be operated under situation 1 as much as possible and it needs

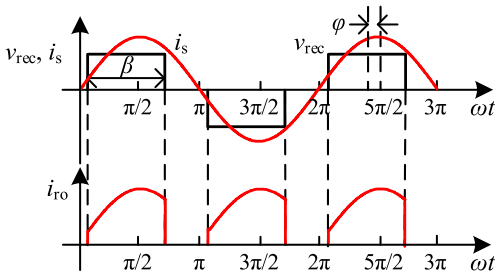

Fig. 9. Waveforms of the input voltage, input current, and output current of the ASPR.

to be avoided to let the ASPR operate in situation 3 where the equivalent load impedance is inductive so that the switching loss can be reduced.

B. Equivalent Impedance Calculation

The receiver rectifier voltage $\dot{V}_{\rm rec}$ is regulated by the ASPR with parameters of the pulse-width β and the phase-shift φ against reference $\dot{I}_{\rm S}$, as shown in Fig. 9. The phase-shift φ indicates the phase difference between the first-harmonic components of $\dot{V}_{\rm rec}$ and $\dot{I}_{\rm S}$. When $\dot{V}_{\rm rec}$ leads $\dot{I}_{\rm S}$, φ is positive and the load provides inductive reactance for the WPT system. Otherwise, it provides capacitive reactance. The magnitude of the first-harmonic components of $\dot{V}_{\rm rec}$ is determined by the pulse-width β and the output voltage V_O. The voltage $\dot{V}_{\rm rec}$ of the ASPR is, thus, provided by

$$\dot{V}_{\rm rec} = \frac{2\sqrt{2}}{\pi} V_O \cdot \sin\left(\frac{\beta}{2}\right) \cdot e^{j\varphi}. \tag{10}$$

According to the waveform of the output current of the ASPR $i_{\rm ro}$ in Fig. 9, the dc output current filtered by the output capacitor $C_{\rm d}$ can be derived by

$$\begin{aligned} I_{\rm O} &= \frac{1}{\pi} \int_{-\varphi+\frac{\pi}{2}-\frac{\beta}{2}}^{-\varphi+\frac{\pi}{2}+\frac{\beta}{2}} \sqrt{2} I_{\rm S} \sin(\omega t)\, d\omega t \\ &= \frac{2\sqrt{2}}{\pi} I_{\rm S} \sin\left(\frac{\beta}{2}\right) \cos\varphi. \end{aligned} \tag{11}$$

By calculating the ratio of $\dot{V}_{\rm rec}$ and $\dot{I}_{\rm S}$, the equivalent impedance of the ASPR can be given as

$$Z_{\rm Leq} = \frac{\dot{V}_{\rm rec}}{\dot{I}_{\rm S}} = R_{\rm Leq} + jX_{\rm Leq} \tag{12}$$

where $R_{\rm Leq}$ and $X_{\rm Leq}$are the equivalent resistance and the reactance of the ASPR, respectively

$$\begin{cases} R_{\rm Leq} = \frac{4}{\pi^2} R_{\rm L} \cos^2(\varphi)\,(1-\cos(\beta)) \\ X_{\rm Leq} = \frac{4}{\pi^2} R_{\rm L} \sin(\varphi)\cos(\varphi)\,(1-\cos(\beta)) \end{cases}. \tag{13}$$

Assuming the load resistrer $R_{\rm L}$ is 30 Ω, the regulation ranges of $R_{\rm Leq}$ and $X_{\rm Leq}$ are shown in Fig. 10 against β and φ. It is clear that with the decreasing of pulse-width β, both the resistance and reactance of ASPR become smaller, while the variation of phase-shift φ has different effect on $R_{\rm Leq}$ and $X_{\rm Leq}$.

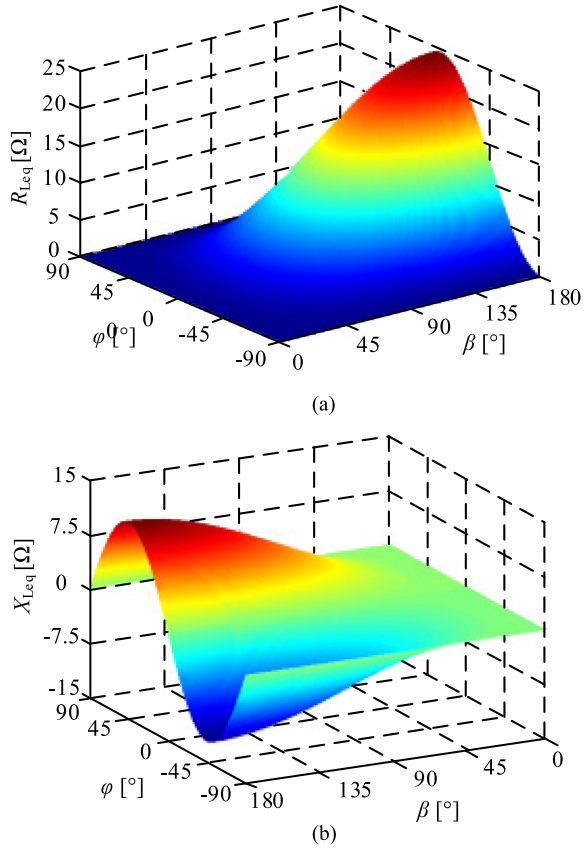

Fig. 10. Regulation ranges of $R_{\rm Leq}$ and $X_{\rm Leq}$ against β and φ. (a) $R_{\rm Leq}$ against β and φ. (b) $X_{\rm Leq}$ against β and φ.

When $\varphi > 0$, $R_{\rm Leq}$ decreases with the increasing of φ, while the absolute value of $X_{\rm Leq}$ increases with φ ranging from 0 to $\pi/4$ and decreases with φ ranging from $\pi/4$ to $\pi/2$. The inductive (capacitive) reactance of the ASPR decreases with the positive (negative) phase-shift φ approaching to zero. Besides, the larger the reactance is required for compensation, the narrower the regulation ranges of $R_{\rm Leq}$ will be, as shown in Fig. 10. The maximum $R_{\rm Leq}$ can reach $8R_L/\pi^2$ when$\beta$is π and φ is zero. The maximum (minimum) $X_{\rm Leq}$ is equal to $4R_L/\pi^2(-4R_L/\pi^2)$ when β is π and φ is $-\pi/4$ $(\pi/4)$. However, the maximum resistance$R_{\rm Leq}$ can only go up to$4R_L/\pi^2$ when the largest reactance $4R_L/\pi^2$ $(-4R_L/\pi^2)$ is provided by the ASPR.

According to (13) and Fig. 10, the pulse-width β and the phase-shift φ are coupled together. The change of β or φ will lead to the alteration of both $R_{\rm Leq}$ and $X_{\rm Leq}$. It needs to decouple the $R_{\rm Leq}$ and $X_{\rm Leq}$ against β or φ in order to get the freedom of controlling $R_{\rm Leq}$ and $X_{\rm Leq}$, separately, which is discussed in the next section.

IV. Proposed Control Strategy

A. Auxiliary Measurement Coil

In the previous section, the factors affecting the system efficiency and the equivalent load impedance have been discussed in detail. Obviously, it is important to have the receiver-side

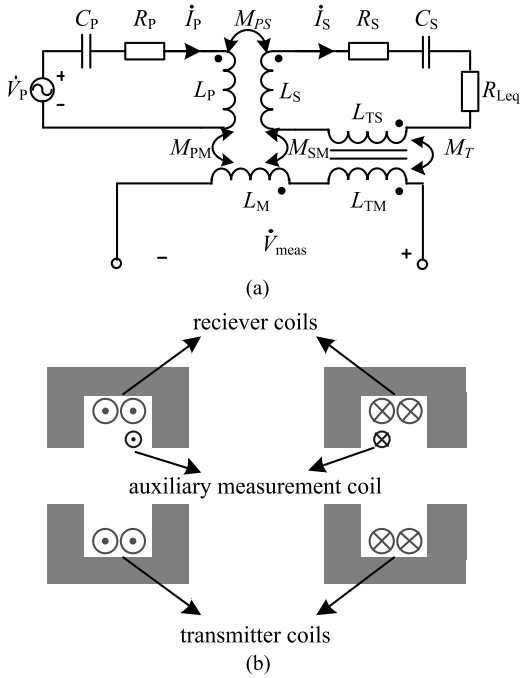

Fig. 11. WPT system with an AMC and a decoupling transformer. (a) Schematic. (b) Structure of the transmitter, receiver, and measurement coil.

resonant by adjusting the reactance provided by the ASPR and the load resistance should be optimal. What should we do next is to find out what the criteria is for the resonant condition of the receiver. The AMC, which is used for synchronization of the bidirectional WPT system in [27], is adopted in this paper to get the phase estimation of the transmitter current. The AMC mounted parallel in the receiver with mutual inductance $M_{\rm SM}$ and $M_{\rm PM}$ is adopted to measure the voltage induced by the currents of the transmitter and receiver, as shown in Fig. 11. Thin wires are suitable for the AMC in which no currents flow. A decoupling transformer with mutual inductance $M_{\rm T} = M_{\rm SM}$ connected with the receiver and the AMC is adopted to cancel out the voltage induced by the receiver-side current $i_{\rm S}$ to the measurement circuit. Then, the equivalent open-circuit voltage in the measurement circuit only remain the induced voltage caused by the transmitter current $i_{\rm P}$ which can be used to justify the resonance condition in the receiver side, as shown in (14). The detailed voltage relationship is derived as follows.

The current of AMC is supposed to be zero as it is an open circuit. Then, the first harmonic of the open-circuit voltage can be expressed according to the basis circuitry analysis as

$$\begin{aligned}\dot{V}_{\rm meas} &= j\omega M_{\rm PM}\dot{I}_{\rm P} + j\omega M_{\rm T}\dot{I}_{\rm S} - j\omega M_{\rm SM}\dot{I}_{\rm S} \\ &= j\omega M_{\rm PM}\dot{I}_{\rm P} + j\omega \dot{I}_{\rm S}(M_{\rm T} - M_{\rm SM}). \end{aligned} \tag{14}$$

As we known, the inductance voltage of the receiver's coil cannot be measured directly by the sensors, but it can be derived from the transmitter current and the mutual inductance between two coils as

$$\dot{V}_{\rm S} = j\omega M_{\rm PS}\dot{I}_{\rm P}. \tag{15}$$

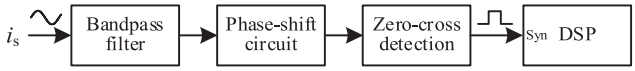

Fig. 12. Generation of the synchronization signal for the ASPR.

By substituting (15) into (14), the open-circuit voltage of the measurement circuit is expressed as

$$\dot{V}_{\rm meas} = \frac{M_{\rm PM}}{M_{\rm PS}}\dot{V}_{\rm S} + j\omega\dot{I}_{\rm S}(M_{\rm T} - M_{\rm SM})\Big|_{M_{\rm T}=M_{\rm SM}} = \frac{M_{\rm PM}}{M_{\rm PS}}\dot{V}_{\rm S}. \tag{16}$$

As long as $M_{\rm T} = M_{\rm SM}$, $\dot{V}_{\rm meas}$ is in phase with the receiver induced voltage $\dot{V}_{\rm S}$. Consequently, $\dot{V}_{\rm meas}$ can be treated as a reference to check whether the receiver side is resonant or not. In other words, when the receiver side is resonant, $\dot{I}_{\rm S}$ and $\dot{V}_{\rm meas}$ are in phase. Otherwise, they are out of phase. The phase difference of the measurement circuit's open-circuit voltage $\dot{V}_{\rm meas}$ and the current of the receiver $\dot{I}_{\rm S}$ can, thus, be employed to indicate the status of nonresonance degree of receiver side.

The influence of the decoupling transformer on the receiver side is quite small. Once the self-inductance $L_{\rm TS}$ of the primary side of the decoupling transformer is considered to be compensated by the receiver resonant capacitor $C_{\rm P}$, $L_{\rm TS}$ has no influence on the resonance condition of the receiver side basically. Meanwhile, the number of turns in the primary side is only 1 or 2. Then, the loss caused by the primary side of the decoupling transformer is ignorable. Besides, no currents exist in the measurement circuit and no impedance is reflected to the receiver side through the decoupling transformer because the secondary side of the decoupling transformer is in an open circuit.

B. Synchronization

In the traditional full-bridge diode rectifier, the diodes switch naturally by the voltage bias when the receiver current crosses zero, but for ASPR, the synchronization between the driving signals of the MOSFETs and the receiver current is required for the phase-shift operation. In this paper, the zero-cross signal of the receiver current is utilized as the synchronization signal, as shown in Fig. 12.

The measurement signal of current $i_{\rm S}$ is captured by a current sensor and passed through a bandpass filter. A phase-shift circuit is then adopted to correct the phase error caused by the detection circuits. After that a zero-cross detection circuit generates the square wave which is in phase with $i_{\rm S}$ to the synchronization input port of the digital signal processor (DSP) to apply the equivalent impedance control strategy of the ASPR.

C. Control Strategy

As discussed above, both the variation of the load and the reactance caused by nonresonance in the receiver side may decrease the system efficiency according to (7). As there are three goals (resonance of the receiver, optimal equivalent resistance, and constant output voltage/current) we are trying to achieve in the application, three degrees of control freedom are needed at least.

According to the topology in Fig. 5, three variables (the pulse width of the inverter, the pulse width, and phase shift of ASPR)

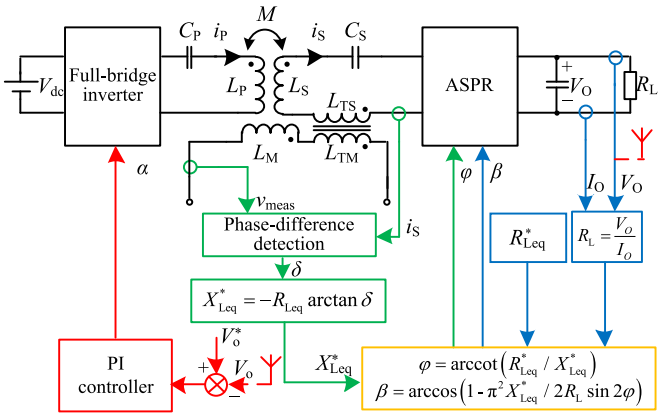

Fig. 13. Control block of the proposed method.

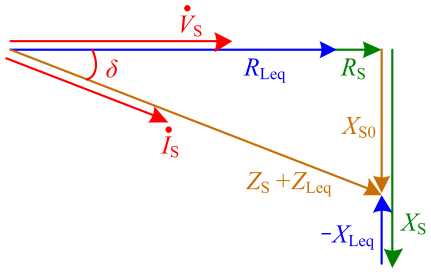

Fig. 14. Impedance triangle in the receiver side.

are selected to be the three degrees of the freedom treated as control parameters in this paper. It is worthy to mention that there are many other variables (methods) can be used as the control variables, alternatively. The method we propose here is one of them. Specifically, the goal of the proposed control strategy is to control the resistance and reactance of equivalent load by ASPR and to regulate the output voltage by the inverter. The control block of the proposed approach to achieve the maximum system efficiency is shown in Fig. 13.

In the receiver-side control loop, the phase difference δ between the induced voltage of the receiver v_S and the receiver current i_S can be measured by detecting the zero-cross signal of i_S and the open-circuit voltage v_{meas} in the phase-difference detection circuit. Fig. 14 shows the relationship of the impedance, the receiver current, and the induced voltage in the receiver side considering δ. According to Fig. 14, the reactance X_{S0} indicating the nonresonance condition in the receiver side can be expressed by

$$X_{S0} = X_S - X_{Leq} \tag{17}$$

where X_S is the reactance of the receiver resonant circuit and X_{Leq} is the instant equivalent reactance of ASPR. X_{S0} can be attained approximately according to R_{Leq} and the detected phase difference δ by

$$\begin{aligned} X_{S0} &= (R_{Leq} + R_S) \tan(\delta) \\ &\approx R_{Leq} \tan(\delta). \end{aligned} \tag{18}$$

In order to cancel X_{S0} and tune the receiver-side circuit, the expected equivalent reactance X^*_{Leq} of ASPR should be

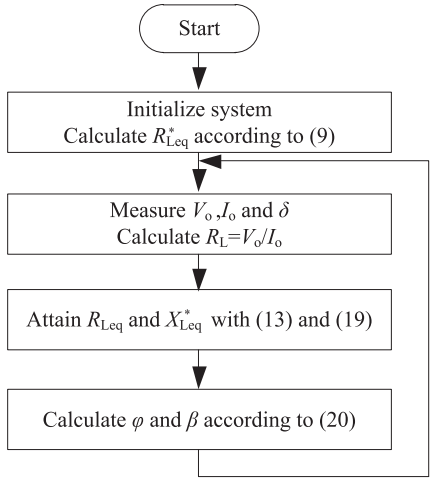

Fig. 15. Flowchart of the control algorithm for ASPR.

equal to

$$X^*_{Leq} = -X_{S0} = -R_{Leq} \arctan(\delta). \tag{19}$$

In addition, the output voltage V_O and output current I_O are measured to estimate the real load R_L. The optimal resistance R^*_{Leq} that ASPR needs to regulate can also be determined accordingly by (9).

However, it is not easy to control the equivalent reactance and resistance of the load independently by altering the phase shift and pulse width of the rectifier independently, as they are coupled by each other. The decoupled method is needed to control the resistance and reactance of the ASPR, separately. Given that R^*_{Leq}, X^*_{Leq}, and R_L are available, the pulse-width β and the phase-shift φ of ASPR can be solved from (13) as

$$\begin{cases} \varphi = \arccot\left(\dfrac{R^*_{Leq}}{X^*_{Leq}}\right) \\ \beta = \arccos\left(1 - \dfrac{\pi^2 X^*_{Leq}}{2R_L \sin 2\varphi}\right) \end{cases}. \tag{20}$$

Based on (20), the equivalent resistance and reactance of the ASPR can be regulated by altering the phase-shift φ and pulse-width β. The control flowchart of $\varphi$and β is shown in Fig. 15.

Generally, the blue and the green closed loops are applied to regulate the equivalent resistance and reactance of the ASPR to make sure that not only the receiver side is resonant but also the equivalent resistance of the load is close to the optimal one. The red closed loop is dedicated to regulate the output voltage/current by adjusting the input voltage. The measured output voltage V_O is transferred to the transmitter-side controller via a wireless communication link. A PI controller is employed to regulate the output voltage by adjusting the pulse-width α of the inverter.

V. Experimental Verifications

A. Prototyping Setup

As shown in Fig. 16, a prototype WPT system is set up to verify the proposed control method according to the parameters listed in Table III. The rate output power is 800 W with

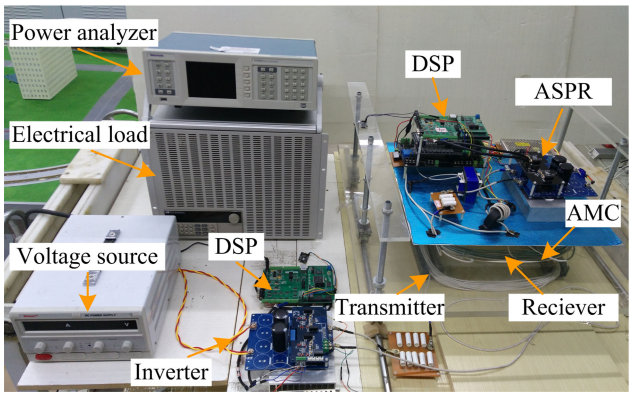

Fig. 16. Experimental prototype.

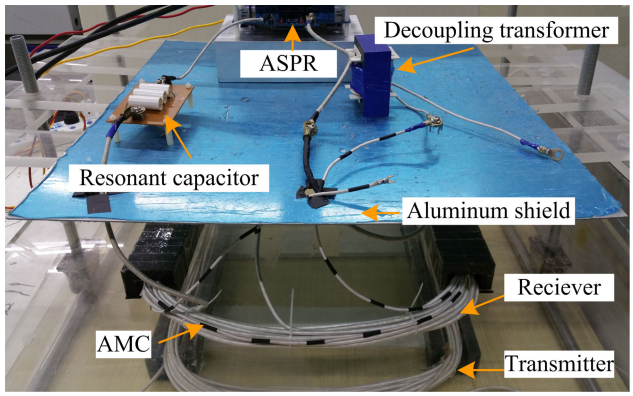

Fig. 17. Installation of AMC and decoupling transformer in the prototype.

TABLE III
PARAMETERS OF THE PROPOSED WPT SYSTEM FOR EXPERIMENTS

Symbol	Parameter	Value	Unit
$U_{\rm dc}$	Input voltage	90	V
f	Inverter frequency	30	kHz
$L_{\rm P}$	Transmitter coil inductance	252	μH
$C_{\rm P}$	Transmitter resonant capacitor	109	nF
$R_{\rm P}$	Transmitter coil ESR	0.1	Ω
$L_{\rm S}$	Receiver coil inductance	246	μH
$C_{\rm S}$	Receiver resonant capacitor	118	nF
$R_{\rm S}$	Receiver coil ESR	0.1	Ω
$L_{\rm m}$	Measurement coil inductance	26.5	μH
$L_{\rm Ts}$	Inductance of the transformer in the receiver side	11.5	μH
$L_{\rm Tm}$	Inductance of the transformer in the measurement side	264.7	μH
$M_{\rm ps}$	Mutual inductance of transmitter and receiver side coils	46.32	μH
$M_{\rm pm}$	Mutual inductance of transmitter and measurement side coils	7.7	μH
$M_{\rm sm}$	Mutual inductance of receiver and measurement side coils	54.9	μH
$M_{\rm T}$	Mutual inductance of the transformer	54.9	μH
$C_{\rm d}$	Output capacitor	940	μF

the 100-V input voltage and 120-V output voltage. The air gap between the transmitter and reciever side is 100 mm. The MOSFETs (IRF640N) are chosen for the full-bridge inverter and the ASPR. The fast-recovery diode (DSEI 2x61-02A) are uesd for the comparision experiments between the ASPR and the passive diode rectifier. The PI controller for regulating the output voltage and the impedance controller of the ASPR are implemented in two seperate DSPs (TMS320F28335) in the transmitter and receicver side. The wireless communication link is implemented by RF modules (nRF24L01). An electric load (IT8518B) serves as the adjustable load resistor. The waveforms are recorded by the oscilloscope (Agilent DSO-X 3034A) and the overall system efficiency is measured by the power analyzer (Tektronix PA3000). Fig. 17 shows the installation of AMC and decoupling transformer in the receiver side. The coil with black dashed line is the measurement coil and the decoupling transformer is on the top of the shield.

B. Experimental Results

The experimental waveforms of the open-circuit voltage $v_{\rm meas}$ in AMC circuit, its zero-cross signal v_{ZM}, the current $i_{\rm S}$ in the receiver side, and its zero-cross signal v_{ZS} in resonance and nonresonance conditions are shown in Fig. 18(a) and (b), respectively. The nonresonance condition is achieved by intentionally setting the receiver-side's capacitor by 10% smaller than the nominal value in resonance. The open-circuit voltage in the AMC circuit is distorted which can be corrected by the bandpass filter in the zero-crossing detector circuit.

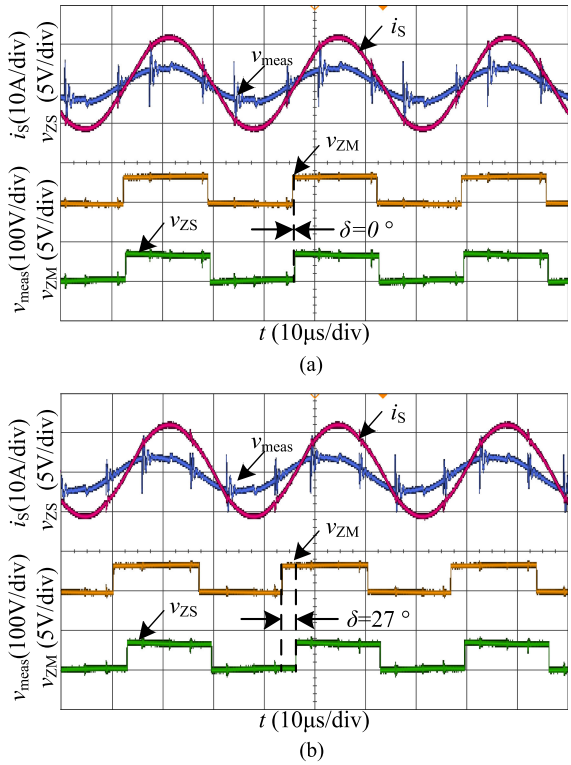

Fig. 18. Open-circuit voltage in the measure coil circuit, the current in the receiver side, and their zero-cross signals. (a) Resonance condition. (b) Nonresonance condition.

In Fig. 18(a), when the receiver side is in resonance, the zero-cross signals of the open-circuit voltage in the measure coil circuit and the current in the receiver side are in phase. When the receiver side is in nonresonance condition, a phase difference between the two zero-cross signals occurs, as shown in Fig. 18(b) so that the phase difference can be adopted to

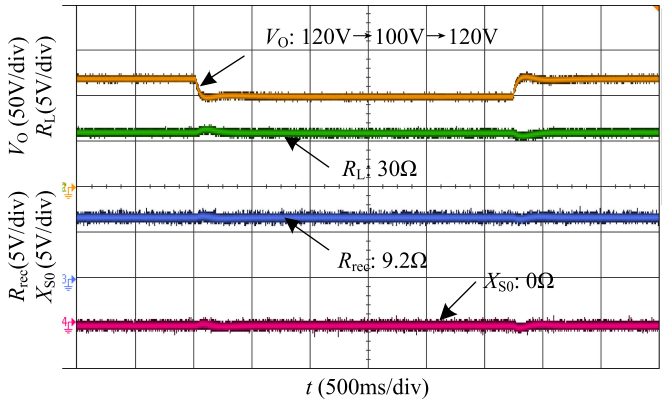

Fig. 19. Time-domain response when output voltage changes.

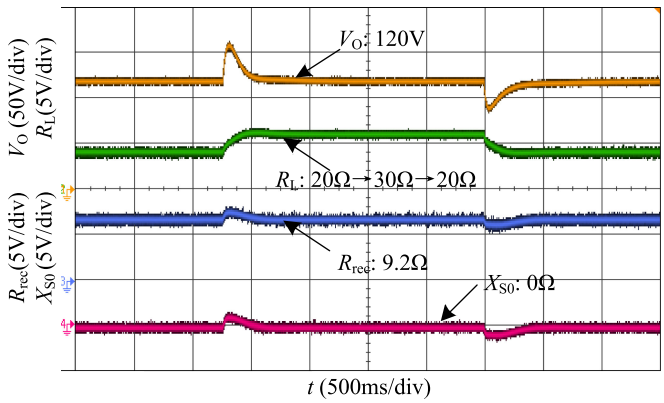

Fig. 20. Time-domain response when load resister changes.

indicate the nonresonance condition of receiver side and calculate the reactance in the receiver side.

Time-domain-response experiments are carried out to evaluate the effectiveness and stability of the proposed method. The value of R_{L}, R_{Leq}, and X_{S0} calculated in the DSP are converted to analog signals by a peripheral digital-to-analog converter module (DAC7724N) connected to the DSP. The numerical value 1 in DSP is converted to 1 V in the analog signal. For the convenience of conversion and observation, the original signals of R_{L}, R_{Leq}, and X_{S0} are multiplied by coefficients 0.2, 0.8, and 2 separately in DSP before the conversion from the DSP to analog output. In the first experiment, the load resister is fixed at 30 Ω. The output voltage is changed from 120 to 100 V and then increased to 120 V again. In the second experiment, the output voltage is fixed at 120 V. The load resister is changed from 20 to 30 Ω and then decreased back to 20 Ω again. The optimal equivalent resistance R^{*}_{Leq} of ASPR is set to 9.2 Ω in both experiments. The results in Figs. 19 and 20 show that, with the proposed method, the output voltage can be regulated as a reference value under the variation conditions of output voltage and load resister, and the equivalent resistance of ASPR can be controlled to be R^{*}_{Leq} (9.2 Ω) and the reactance X_{S0} in the receiver side is nearly zero.

In order to verify the performance of the proposed method, another two methods are employed to be compared under various conditions.

1) *Optimal load resistance control (OLRC) method:* As analyzed in Section II, an optimal load resistance value exists for the maximum efficiency point of the system. If the system is assumed to be fine -tuned, the optimal load resistance can be achieved by adjusting the pulse width of the rectifier with no phase shift related to the receiver current compared to the proposed method. Thus, the OLRC method controls the equivalent resistance of the active rectifier as $R_{\mathrm{Leq}} = R^{\mathrm{opt}}_{\mathrm{Leq}} = \sqrt{R_{\mathrm{S}}(M^2\omega^2 + R_{\mathrm{P}}R_{\mathrm{S}})/R_{\mathrm{P}}}$ by adjusting the pulse width of the rectifier.
2) *Passive diode rectifier:* In this method, the ASPR is replaced with passive diode rectifier. Because the diode is conducted by the forwards voltage bias, neither the pulse width nor the phase shift of the rectifier is adjustable. The equivalent resistance of the diode rectifier equals $8R_{\mathrm{L}}/\pi^2$.

The comparison experiments are carried out under the following conditions: 1) the dc input voltage is fixed at 100 V and the dc output voltage is regulated as 120 V by adjusting the pulse width of the inverter; 2) the transmitter side's current I_{P} is limited to 11 A to avoid overcurrent in resonant capacitor; and 3) the output power is changed by adjusting the dc load resister R_{L}.

Fig. 21 shows the characteristic waveforms of the inverter and the rectifier with the three methods. Because an OLRC method only changes the equivalent resistance R_{Leq} of the rectifier and the diode rectifier method changes nothing, the reactance caused by the nonresonance condition in the receiver side still exists with the two methods. The reflected impedance of the receiver in the transmitter side is not pure resistance which leads to out of phase between the output current i_{P} and output voltage v_{inv} of the inverter, as shown in Fig. 21(b), (c), (e), and (f). The experimental waveforms adopting the proposed method where both the pulse width and the phase shift of ASPR are adjusted are shown in Fig. 21(a) and (d). The input current i_{S} and input voltage v_{rec} of the rectifier are not in phase in order to provide extra reactance to compensate the passive reactance, which leads to the nonresonance condition in the receiver side. According to (9), (20), β and φ can be calculated as 119.3° and 29.8° theoretically when the output power is 750 W and are measured as 120.1° and 29.1° in Fig. 21(a). When the output power is 300 W, β and φ can be calculated as 66.2° and 29.8°, respectively, and are measured as 67° and 29.1° in Fig. 21(d). Then, the reflected impedance of the receiver in the transmitter side is close to pure resistance. As a result, the output current i_{P} and output voltage v_{inv} of the inverter are in phase as shown in Fig. 21(a) and (d).

The overall system efficiency of the three methods is compared in Fig. 22 with output power ranging from 300 to 800 W. The system efficiency with the proposed method is greater than 91% in all load conditions. Obviously, the proposed method can dramatically improve the efficiency compared with the traditional diode rectifier by 2% in heavy load and 10% in light load. So does OLRC method. The efficiency improvement compared to the diode method owes to the equivalent resistance R_{Leq} control in the proposed method and OLRC method. The two methods adjust R_{Leq} to be $R^{\mathrm{opt}}_{\mathrm{Leq}}$ in (9) under various load condition. Besides, compared with OLRC, the proposed method can

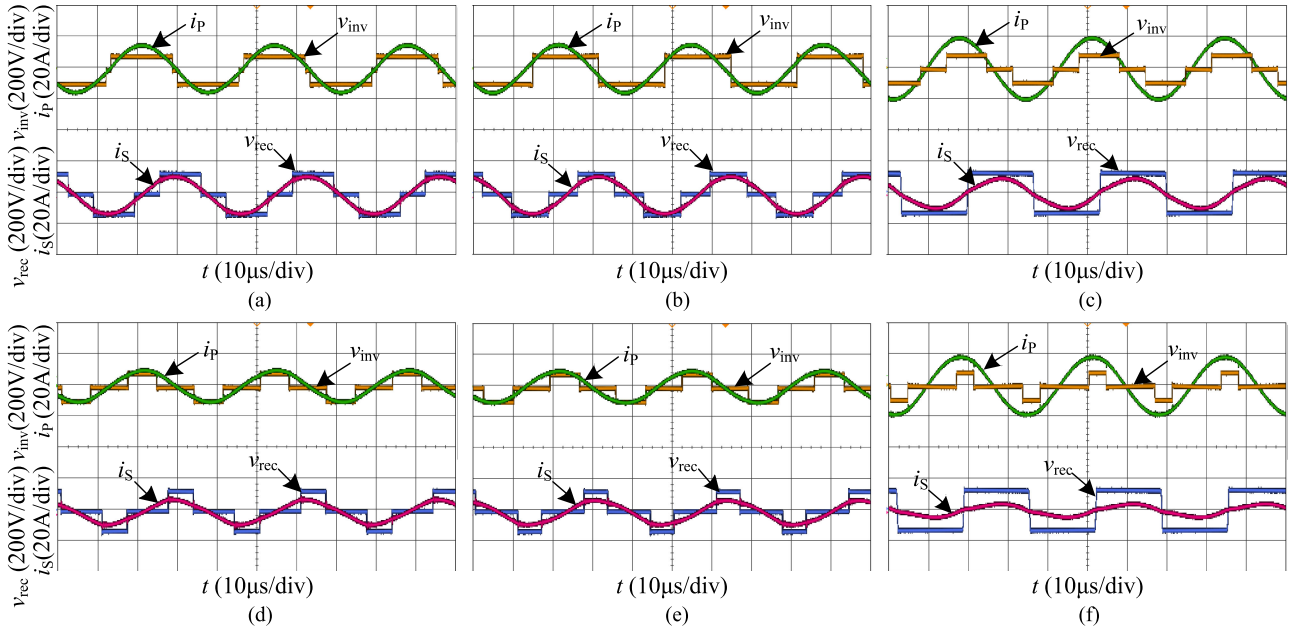

Fig. 21. Characteristic waveforms of the inverter and rectifier with three methods. (a) Proposed method with 750-W output power. (b) OLRC with 750-W output power. (c) Diode rectifier with 750-W output power. (d) Proposed method with 300-W output power. (e) OLRC with 300-W output power. (f) Diode rectifier with 300-W output power.

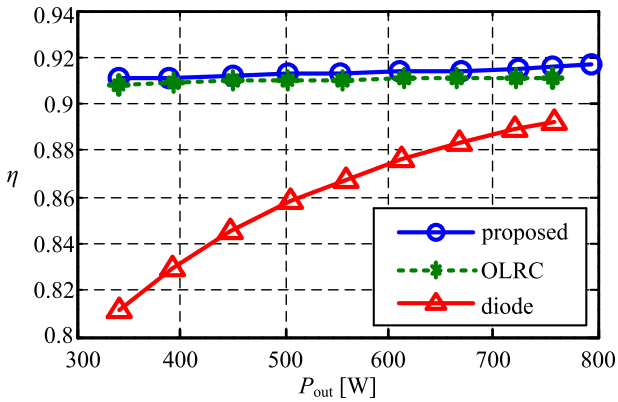

Fig. 22. Overall system efficiency comparison among the proposed method, the OLRC, and the diode rectifier with different output power.

further improve the system efficiency by 0.6% because ASPR can generate X_{Leq} to compensate X_{S} and tune the receiver side while optimizing the equivalent resistance R_{Leq}. For the OLRC method, only the pulse width of the rectifier is adjusted to optimize the equivalent resistance R_{Leq}. As no equivalent reactance of the rectifier is provided, no matter what the pulse width of the rectifier is, X_{S} exists and η is reduced accordingly against X_{S} as analyzed in Fig. 4. Generally, the proposed method which benefits from the two degree of control freedom, the pulse width and the phase shift of the ASPR, can improve the system efficiency by tuning the receiver side and optimizing the load resistance.

The other important observation from the results is that compared to OLRC and the diode method, the proposed method can also improve the power transfer capability with restricted transmitter current I_P. When I_P is limited to 11 A, the maximum output power of the system with OLRC is only 757 W, while the system with the proposed method is 796 W which is 5% larger than that of OLRC. The reason is that X_{S} in the receiver side is compensated with the proposed method while it cannot be canceled with an OLCR method. According to Fig. 3, if X_{S} exists, the output voltage is lower than that in the resonant condition with the same I_P. Therefore, more power can be transferred to the load with the proposed method than that of the OLCR with a given I_P.

VI. Conclusion

An ASPR-based optimal reactance and resistance control strategy with an AMC is proposed in this paper to track the maximum efficiency point under varied load and detuning conditions. By detecting the open-circuit voltage of the AMC circuit, the phase of the induced voltage in the receiver side can be measured and then the reactance caused by detuning can be calculated in real time. Two controllable variables: the pulse width and phase shift of the ASPR are adopted to tune the receiver side and control the equivalent load resistance to be the optimal value. At the same time, the power-source inverter is available to regulate the output voltage/current. The proposed control method is validated by comparison experiments with an OLRC method and the passive diode rectifier. When the capacitor tolerance in the receiver side is 10%, the system efficiency is 91.7% by applying the proposed control method at rated output power which is 2% higher than the diode rectifier and 0.6% for the OLRC method. Meanwhile, the proposed method can improve the output power capacity by 5% compared with the OLRC method. Various load conditions have been applied to verify the performance of the proposed method.

REFERENCES

[1] Y. Li, R. Mai, L. Lu, and Z. He, "Active and reactive currents decomposition based control of angle and magnitude of current for a parallel multi-inverter IPT system," *IEEE Trans. Power Electron.*, vol. 32, no. 2, pp. 1602–1614, Feb. 2017.

[2] A. Dukju and H. Songcheol, "Wireless power transmission with self-regulated output voltage for biomedical implant," *IEEE Trans. Ind. Electron.*, vol. 61, no. 5, pp. 2225–2235, May 2014.

[3] Z. Cheng, Y. Lei, K. Song, and C. Zhu, "Design and loss analysis of loosely coupled transformer for an underwater high-power inductive power transfer system," *IEEE Trans. Magn.*, vol. 51, no. 7, pp. 1–10, Jul. 2015.

[4] J. Yungtaek and M. M. Jovanovic, "A contactless electrical energy transmission system for portable-telephone battery chargers," *IEEE Trans. Ind. Electron.*, vol. 50, no. 3, pp. 520–527, Jun. 2003.

[5] J. Deng, W. Li, T. D. Nguyen, S. Li, and C. C. Mi, "Compact and efficient bipolar coupler for wireless power chargers: Design and analysis," *IEEE Trans. Power Electron.*, vol. 30, no. 11, pp. 6130–6140, Nov. 2015.

[6] C. Zheng *et al.*, "High-efficiency contactless power transfer system for electric vehicle battery charging application," *IEEE J. Emerg. Sel. Topics Power Electron.*, vol. 3, no. 1, pp. 65–74, Mar. 2015.

[7] S. Y. Choi, B. W. Gu, S. Y. Jeong, and C. T. Rim, "Advances in wireless power transfer systems for roadway-powered electric vehicles," *IEEE J. Emerg. Sel. Topics Power Electron.*, vol. 3, no. 1, pp. 18–36, Mar. 2015.

[8] J. T. Boys and G. A. Covic, "The inductive power transfer story at the University of Auckland," *IEEE Circuits Syst. Mag.*, vol. 15, no. 2, pp. 6–27, May 2015.

[9] J. M. Miller, P. T. Jones, J. Li, and O. C. Onar, "ORNL experience and challenges facing dynamic wireless power charging of EV's," *IEEE Circuits Syst. Mag.*, vol. 15, no. 2, pp. 40–53, May 2015.

[10] K. Ukita, T. Kashiwagi, Y. Sakamoto, and T. Sasakawa, "Evaluation of a non-contact power supply system with a figure-of-eight coil for railway vehicles," in *2015 IEEE PELS Workshop Emerg. Technol., Wireless Power*, Jun. 2015, pp. 1–6.

[11] J. H. Kim *et al.*, "Development of 1-MW inductive power transfer system for a high-speed train," *IEEE Trans. Ind. Electron.*, vol. 62, no. 10, pp. 6242–6250, Oct. 2015.

[12] R. Xue, K. Cheng, and M. Je, "High-efficiency wireless power transfer for biomedical implants by optimal resonant load transformation," *IEEE Trans. Circuits Syst. I, Reg. Papers*, vol. 60, no. 4, pp. 867–874, Apr. 2013.

[13] S. Y. R. Hui, W. Zhong, and C. K. Lee, "A critical review of recent progress in mid-range wireless power transfer," *IEEE Trans. Power Electron.*, vol. 29, no. 9, pp. 4500–4511, Sep. 2014.

[14] W. Zhang, S. Wong, C. K. Tse, and Q. Chen, "Design for efficiency optimization and voltage controllability of series–series compensated inductive power transfer systems," *IEEE Trans. Power Electron.*, vol. 29, no. 1, pp. 191–200, Jan. 2014.

[15] L. Chen, S. Liu, Y. C. Zhou, and T. J. Cui, "An optimizable circuit structure for high-efficiency wireless power transfer," *IEEE Trans. Ind. Electron.*, vol. 60, no. 1, pp. 339–349, Jan. 2013.

[16] W. Zhang, S. Wong, C. K. Tse, and Q. Chen, "Load-independent duality of current and voltage outputs of a series- or parallel-compensated inductive power transfer converter with optimized efficiency," *IEEE J. Emerg. Sel. Topics Power Electron.*, vol. 3, no. 1, pp. 137–146, Mar. 2015.

[17] G. Buja, M. Bertoluzzo, and K. N. Mude, "Design and experimentation of WPT charger for electric city car," *IEEE Trans. Ind. Electron.*, vol. 62, no. 12, pp. 7436–7447, Dec. 2015.

[18] T. Diekhans and R. W. De Doncker, "A dual-side controlled inductive power transfer system optimized for large coupling factor variations and partial load," *IEEE Trans. Power Electron.*, vol. 30, no. 11, pp. 6320–6328, Nov. 2015.

[19] A. Berger, M. Agostinelli, S. Vesti, J. A. Oliver, J. A. Cobos, and M. Huemer, "A wireless charging system applying phase-shift and amplitude control to maximize efficiency and extractable power," *IEEE Trans. Power Electron.*, vol. 30, no. 11, pp. 6338–6348, Nov. 2015.

[20] D. Kobayashi, T. Imura, and Y. Hori, "Real-time coupling coefficient estimation and maximum efficiency control on dynamic wireless power transfer for electric vehicles," in *Proc. 2015 IEEE PELS Workshop Emerg. Technol, Wireless Power*, Jun. 2015, pp. 1–6.

[21] H. Li, J. Li, K. Wang, W. Chen, and X. Yang, "A maximum efficiency point tracking control scheme for wireless power transfer systems using magnetic resonant coupling," *IEEE Trans. Power Electron.*, vol. 30, no. 7, pp. 3998–4008, Jul. 2015.

[22] W. X. Zhong and S. Y. R. Hui, "Maximum energy efficiency tracking for wireless power transfer systems," *IEEE Trans. Power Electron.*, vol. 30, no. 7, pp. 4025–4034, Jul. 2015.

[23] M. Fu, H. Yin, X. Zhu, and C. Ma, "Analysis and tracking of optimal load in wireless power transfer systems," *IEEE Trans. Power Electron.*, vol. 30, no. 7, pp. 3952–3963, Jul. 2015.

[24] T. C. Beh, M. Kato, T. Imura, S. Oh, and Y. Hori, "Automated impedance matching system for robust wireless power transfer via magnetic resonance coupling," *IEEE Trans. Ind. Electron.*, vol. 60, no. 9, pp. 3689–3698, Sep. 2013.

[25] Z. Dang and J. A. Abu Qahouq, "Extended-Range Two-coil Adaptively Reconfigurable Wireless Power Transfer System," in *Proc. Ann. IEEE Appl. Power Electron. Conf. Exposition*, Mar. 2015, pp. 1630–1636.

[26] K. Colak, E. Asa, M. Bojarski, D. Czarkowski, and O. C. Onar, "A novel phase-shift control of semibridgeless active rectifier for wireless power transfer," *IEEE Trans. Power Electron.*, vol. 30, no. 11, pp. 6288–6297, Nov. 2015.

[27] D. J. Thrimawithana, U. K. Madawala, and M. Neath, "A synchronization technique for bidirectional IPT systems," *IEEE Trans. Ind. Electron.*, vol. 60, no. 1, pp. 301–309, Jan. 2013.

Ruikun Mai (M'14) received the B.Sc. and Ph.D. degrees from the School of Electrical Engineering, Southwest Jiaotong University, Chengdu, China, in 2004 and 2010, respectively.

He is currently an Associate Professor with the School of Electrical Engineering, Southwest Jiaotong University. His research interests include wireless power transfer and its application in railway systems, power system stability, and control.

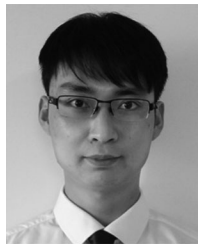

Yeran Liu (S'17) received the B.Sc. degree from the School of Electrical Engineering, Southwest Jiaotong University E'mei Campus, E'mei, China, in 2015. He is currently working toward the Ph.D. degree at the School of Electrical Engineering, Southwest Jiaotong University, Chengdu, China.

His research focuses on wireless power transfer.

Yong Li (S'15) received the B.Sc. degree from the School of Electrical Engineering, Southwest Jiaotong University, Chengdu, China, in 2013, where he is currently working toward the Ph.D. degree.

His main research interests include wireless power transfer and resonant converters.

Pengfei Yue received the B.Sc. degree from the School of Electrical Engineering and Automation, Henan Polytechnic University, Jiaozuo, China, in 2016. He is currently working toward the M.Sc. degree at the School of Electrical Engineering, Southwest Jiaotong University, Chengdu, China.

His research focuses on wireless power transfer.

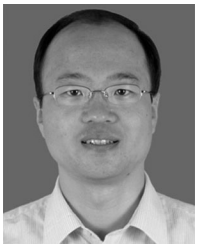

Guangzhong Cao (M'15) received the B.Sc., M.Sc., and Ph.D. degrees in electrical engineering and automation from Xi'an Jiaotong University, Xi'an, China, in 1989, 1992, and 1996, respectively.

He is currently a Professor and Director with Shenzhen Key Laboratory of Electromagnetic Control, Shenzhen University, Shenzhen, China. He has authored more than 90 articles in refereed journals and conferences. His research interests include motor control, and control theory and its application.

Zhengyou He (M'10–SM'13) received the B.Sc. degree and the M.Sc. degree in computational mechanics from Chongqing University, Chongqing, China, in 1992 and 1995, respectively, and the Ph.D. degree from the School of Electrical Engineering, Southwest Jiaotong University, Chengdu, China, in 2001.

He is currently a Professor with the School of Electrical Engineering, Southwest Jiaotong University. His research interests include signal process and information theory applied to electrical power system, and application of wavelet transforms in power system.